

Gamow-Teller strength distributions at finite temperatures and electron capture in stellar environments

Alan A. Dzhioev,^{1,*} A. I. Vdovin,¹ V. Yu. Ponomarev,² J. Wambach,^{2,3} K. Langanke,^{3,2,4} and G. Martínez-Pinedo³

¹*Bogoliubov Laboratory of Theoretical Physics, JINR, 141980, Dubna, Russia*

²*Institut für Kernphysik, Technische Universität Darmstadt, 64289 Darmstadt, Germany*

³*GSI Helmholtzzentrum für Schwerionenforschung, Planckstr. 1, 64291 Darmstadt, Germany*

⁴*Frankfurt Institute for Advanced Studies, Ruth-Moufang-Str. 1, 60438 Frankfurt, Germany*

(Dated: November 2, 2018)

We propose a new method to calculate stellar weak-interaction rates. It is based on the Thermo-Field-Dynamics formalism and allows the calculation of the weak-interaction response of nuclei at finite temperatures. The thermal evolution of the GT_+ distributions is presented for the sample nuclei $^{54,56}\text{Fe}$ and $^{76,78,80}\text{Ge}$. For Ge we also calculate the strength distribution of first-forbidden transitions. We show that thermal effects shift the GT_+ centroid to lower excitation energies and make possible negative- and low-energy transitions. In our model we demonstrate that the unblocking effect for GT_+ transitions in neutron-rich nuclei is sensitive to increasing temperature. The results are used to calculate electron capture rates and are compared to those obtained from the shell model.

PACS numbers: 26.50.+x, 23.40.-s, 21.60.Jz, 24.10.Pa

I. INTRODUCTION

The properties of nuclei at finite temperatures have attracted attention for a long time. Due to a considerable amount of experimental data the main subject of the study was the thermal properties of the giant dipole resonance (see, e.g., [1, 2] and reference therein). In the astrophysical context the thermal properties of Gamow-Teller (GT) transitions are of special interest since they play a crucial role in weak-interaction mediated reactions (electron capture, beta-decay, neutrino scattering etc.) [3]. For example, electron capture on iron group nuclei initiates the gravitational collapse of the core of a massive star triggering supernova explosions. Moreover, electron capture rates largely determine the mass of the core and thus the fate of the shock wave formed by the supernova explosion. Since the strong phase space dependence makes the relevant stellar weak-interaction rates at the early stage of the collapse – when the electron chemical potential μ_e is of the same order as the nuclear Q -values – very sensitive to the GT distributions these need to be calculated very accurately in this regime. With proceeding collapse and hence increasing density, μ_e grows faster than the Q -values of the nuclei present in the matter composition, the capture rates become less sensitive to the details of the GT distribution and are mainly determined by the total GT strength and its centroid energy. However, forbidden transitions can no longer be neglected when μ_e reaches values of the order of 30 MeV at core densities $\rho > 10^{11}$ g/cm³ [3, 4]. The situation is further complicated by the fact that weak-interaction processes in stellar environments take place at temperatures of the order a few hundred keV to a few MeV and GT transitions occur not

only from the nuclear ground state, but also from excited states.

From a microscopic point of view, there are two routes of handling GT strength distributions and weak-interaction rates at finite temperatures. One is a state-by-state evaluation of the rate by summing over Boltzmann-weighted, individually determined GT strengths for the various states. The second is based on an equilibrium statistical formulation of the nuclear many-body problem. In this approach, the thermal response of a nucleus to an external perturbing field is given by the canonical (or grand canonical) expectation value of the corresponding transition operator. When applied to charge-exchange processes this method yields the temperature-dependent GT and first forbidden strength function that can be then used to calculate weak-interaction rates.

For *sd* and *pf*-shell nuclei the first approach was originally used by Fuller et al. [5] who calculated stellar weak-interaction rates using the independent-particle shell-model, supplemented by experimental data, whenever available. To allow for GT transitions from nuclear excited states these authors employed the Brink hypothesis. This assumes that the GT strength distribution on excited states is the same as for the ground state, only shifted by the excitation energy of the state. These rates were subsequently updated, taking into account the quenching of axial coupling constant [6]. Modern high-performance computing capabilities combined with state-of-the-art diagonalization approaches make possible shell-model calculations of the GT strength distribution not only for the nuclear ground state, but also for the few lowest excited states. It was demonstrated [7, 8] that even for the lowest excited states in the parent nucleus the Brink hypothesis is valid only for the bulk of the GT strength, but is not applicable for the individual transitions to states at low-excitation energy in the

*dzhioev@theor.jinr.ru

daughter nucleus. Taking this into account, the weak-interaction rates based on the shell-model diagonalization approach [9, 10] were derived from the individual GT distributions from the lowest excited states and from 'back-resonant contributions', i.e. from transitions determined from the inverse GT distributions connecting excited states in the daughter to the lowest states in the parent spectrum. However, the compilation of [9, 10] applied Brink's hypothesis when taking into account GT transitions from highly excited states. Weak-interaction rates have also been computed using the spectral distribution theory [11] and the proton-neutron quasiparticle RPA model [12]. The first method is also based on the Brink hypothesis. The latter does not use this hypothesis, but some uncertainties arise due to the approximate treatment of the parent excited states as multi-quasiparticle states as well as the insufficient knowledge of the quantum numbers of the states involved. Recently stellar electron capture rates have been calculated within the framework of the finite temperature RPA using a set of Skyrme interactions [13]. This method has the advantage of consistency, however, it misses relevant correlations which, as we will demonstrate in the present paper, are crucial to derive stellar electron capture rates for neutron-rich nuclei.

The statistical way for the calculation of temperature-dependent GT and first-forbidden strength functions was first applied in [4] to study electron capture on neutron-rich nuclei. The most advances realization of this way is presently performed in the framework of the shell-model Monte-Carlo (SMMC) method [14]. It was found [15] that with increasing temperature the GT centroids shift to lower excitation energies and the widths of the distributions increase with the appearance of low-lying strength. Both effects arise from thermally excited states, i.e., the Brink hypothesis is not supported by SMMC calculations. In spite of its advantages, the SMMC method only yields the lowest moments of the GT strength distributions which introduce some inaccuracies into the rate calculations. Moreover, the SMMC method has restrictions in its applicability to odd-odd and odd-A nuclei at low temperatures.

Thus, the problem of an accurate description of the GT strength distribution at finite temperatures and reliable estimates of stellar weak-interaction rates is not solved completely yet: The shell-model diagonalization approach allows for detailed spectroscopy, but partially employs the Brink hypothesis. The SMMC method is free from this disadvantage, but cannot provide a detailed strength distribution. Moreover, present computer capabilities allow the application of the shell-model diagonalization method only to nuclei in the iron region ($A = 45 - 65$), whereas the SMMC approach can in principle be applied to all nuclei. However, such calculations are rather time-consuming and have therefore been limited to about 200 nuclei with mass numbers $A = 65 - 120$ [3, 16], while weak processes in more massive and neutron-rich nuclei also play an important role

in various astrophysical scenarios. Therefore, alternative methods to deal with Gamow-Teller strength distributions and weak-interaction rates at finite temperatures are desirable.

In this paper we study the temperature dependence of the Gamow-Teller strength applying the proton-neutron quasiparticle RPA [17] extended to finite temperature by the Thermo-Field-Dynamics (TFD) formalism [18, 19]. This technique has the advantage that it does not rely on Brink's hypothesis. The energies of the GT transitions and corresponding transition strengths are calculated as functions of the nuclear temperature. In this paper, we apply this method for the calculations of weak-interaction rates on iron group nuclei and neutron-rich nuclei beyond *pf*-shell. However, this method is not only restricted to these nuclei but can be applied to heavier nuclei as well. In addition, it allows calculations of the strength distributions for forbidden transitions which contribute significantly to weak-interaction rates at high densities. Although, in the present paper, we restrict our study to the one-phonon approach, the method can be extended to higher phonon admixtures thus yielding more detailed strength distributions.

The paper is organized as follows. In Sec. II, some important features of the TFD formalism with application to the nuclear structure problem at finite temperatures are presented. The finite temperature (TQRPA) equations, which describe the strength distribution of charge-exchange transitions in hot nuclei, are given in this section as well. In Sec. III the necessary formulae to calculate electron capture rates in a stellar environment are introduced. Results for the GT strength distributions and electron capture rates in $^{54, 56}\text{Fe}$ are presented in Sec. IV. Here, we also compare the results with those from the shell-model diagonalization approach. In Sec. V, we study the temperature dependence of GT and first-forbidden strength distributions in the neutron-rich isotope ^{76}Ge . The corresponding electron capture cross sections and rates are calculated and compared with those obtained based on a hybrid SMMC+RPA model [20]. Conclusions are drawn in Sec. VI.

II. FORMALISM

As a method to study a thermal behavior of quantum many-body systems the TFD method has two attractive features: a) temperature effects arise explicitly as T -dependent vertices, providing a convenient starting point for various approximations; b) temperature and time are independent variables. The first feature allows for straightforward extensions of well-established zero-temperature approximations. It has been employed previously in [21, 22, 23, 24, 25] where selected nuclear structure problems at finite temperatures were considered.

The standard TFD formalism treats a many-particle system in thermal equilibrium with a heat bath and a particle reservoir in the grand canonical ensemble.

The thermal average of a given operator A is calculated as the expectation value in a specially constructed, temperature-dependent state $|0(T)\rangle$, which is termed the thermal vacuum. This expectation value is equal to the usual grand canonical average of A .

To construct the state $|0(T)\rangle$, a formal doubling of the system degrees of freedom is introduced. In TFD, a tilde conjugate operator \tilde{A} – acting in the independent Hilbert space – is associated with A , in accordance with properly formulated tilde conjugation rules [18, 19, 26]. For a system governed by the Hamiltonian H the whole Hilbert space is now spanned by the direct product of the eigenstates of H ($H|n\rangle = E_n|n\rangle$) and those of the tilde Hamiltonian \tilde{H} , both having the same eigenvalues ($\tilde{H}|\tilde{n}\rangle = E_n|\tilde{n}\rangle$). In the doubled Hilbert space, the thermal vacuum is defined as the zero-energy eigenstate of the so-called thermal Hamiltonian $\mathcal{H} = H - \tilde{H}$ and it satisfies the thermal state condition [18, 19, 26]

$$A|0(T)\rangle = \sigma e^{\mathcal{H}/2T} \tilde{A}^\dagger |0(T)\rangle, \quad (1)$$

where $\sigma = 1$ for bosonic A and $\sigma = i$ for fermionic A .

The important point is that in the doubled Hilbert space the time-translation operator is not the initial Hamiltonian H , but the thermal Hamiltonian \mathcal{H} . This means that the excitations of the thermal system are obtained by the diagonalization of \mathcal{H} . As it follows from the definition of \mathcal{H} each of its eigenstates with positive energy has a counterpart – the tilde-conjugate eigenstate – with negative energy, but the same absolute value. This is a way to treat excitation- and de-excitation processes at finite temperatures within TFD.

Obviously, in most of practical cases one cannot diagonalize \mathcal{H} exactly. Usually, one resorts to certain approximations such as the Hartree-Fock Bogoliubov mean field theory (HFB) and the Random-Phase Approximation (RPA) (see e.g. [22]). In what follows the formal part of the TFD studies for charge-exchange excitations in hot nuclei is based in part on the results of [27, 28].

In our present study we use a phenomenological nuclear Hamiltonian consisting of a static mean field, BCS pairing interactions and separable multipole and spin-multipole particle-hole interactions, including isoscalar and isovector parts. This is usually referred to as the quasiparticle-phonon model (QPM) [29]. It was used to study the charge-exchange excitations in nuclei at zero temperature in [30, 31]. In principle, the QPM formalism enables one to go beyond the QRPA and take into account the coupling of quasiparticles and phonons. At finite temperatures this coupling was considered in [24, 27]. However, in the present study we restrict ourselves to the thermal QRPA.

The main line of the present discussion is very similar to the QPM at $T = 0$ [29]. We begin with the thermal Hamiltonian, which reads as

$$\mathcal{H}_{\text{QPM}} = H_{\text{QPM}} - \tilde{H}_{\text{QPM}} = \mathcal{H}_{\text{sp}} + \mathcal{H}_{\text{pair}} + \mathcal{H}_{\text{ph}}. \quad (2)$$

The first step in the approximate diagonalization of \mathcal{H}_{QPM} is the treatment of the pairing correlations. This

is done by two successive unitary transformations. The first is the usual Bogoliubov u, v transformation from the original particle operators a_{jm}^\dagger, a_{jm} to the quasiparticle ones $\alpha_{jm}^\dagger, \alpha_{jm}$. The same transformation is applied to tilde operators $\tilde{a}_{jm}^\dagger, \tilde{a}_{jm}$, thus producing the tilde quasiparticle operators $\tilde{\alpha}_{jm}^\dagger, \tilde{\alpha}_{jm}$.

The second transformation is the so-called thermal Bogoliubov transformation [18, 19]. It mixes the quasiparticle and tilde quasiparticle operators, thus producing thermal quasiparticle operators and their tilde partners: $\beta_{jm}^\dagger, \beta_{jm}, \tilde{\beta}_{jm}^\dagger, \tilde{\beta}_{jm}$. We use Ojima's [26] complex form of the thermal Bogoliubov transformation

$$\begin{aligned} \beta_{jm}^\dagger &= x_j \alpha_{jm}^\dagger - i y_j \tilde{\alpha}_{jm}, \\ \tilde{\beta}_{jm}^\dagger &= x_j \tilde{\alpha}_{jm}^\dagger + i y_j \alpha_{jm}, \quad (x_j^2 + y_j^2 = 1). \end{aligned} \quad (3)$$

The reasons for this are given in [27].

The coefficients u_j, v_j, x_j, y_j are found by diagonalizing $\mathcal{H}_{\text{sp}} + \mathcal{H}_{\text{pair}}$ and demanding that the vacuum of thermal quasiparticle obeys the thermal state condition (1). This is equivalent to the minimization of the thermodynamic potential for Bogoliubov quasiparticles. As a result one obtains the following equations for u_j, v_j and x_j, y_j :

$$v_j = \frac{1}{\sqrt{2}} \left(1 - \frac{E_j - \lambda_\tau}{\varepsilon_j} \right)^{1/2}, \quad u_j = (1 - v_j^2)^{1/2}, \quad (4)$$

$$y_j = \left[1 + \exp\left(\frac{\varepsilon_j}{T}\right) \right]^{-1/2}, \quad x_j = (1 - y_j^2)^{1/2}, \quad (5)$$

where $\varepsilon_j = \sqrt{(E_j - \lambda_\tau)^2 + \Delta_\tau^2}$ and τ is the isospin quantum number $\tau = n, p$.

The pairing gap Δ_τ and the chemical potential λ_τ are the solutions to the finite-temperature BCS equations

$$\begin{aligned} \Delta_\tau(T) &= \frac{G_\tau}{2} \sum_j^\tau (2j+1)(1 - 2y_j^2)u_j v_j, \\ N_\tau &= \sum_j^\tau (2j+1)(v_j^2 x_j^2 + u_j^2 y_j^2), \end{aligned} \quad (6)$$

where N_τ is the number of neutrons or protons in a nucleus and \sum^τ implies a summation over neutron or proton single-particle states only. From the numerical solution of Eqs. (6) it is found that the (pseudo)critical temperature is $T_{\text{cr}} \approx \frac{1}{2}\Delta_\tau(0)$ (see e.g. [32, 33]) in accordance with the BCS theory.

With the coefficients u_j, v_j, x_j, y_j , defined by Eqs. (4, 5), the one-body part of $\mathcal{H}_{\text{sp}} + \mathcal{H}_{\text{pair}}$ reads

$$\mathcal{H}_{\text{sp}} + \mathcal{H}_{\text{pair}} \simeq \sum_\tau \sum_{jm}^\tau \varepsilon_j (\beta_{jm}^\dagger \beta_{jm} - \tilde{\beta}_{jm}^\dagger \tilde{\beta}_{jm}) \quad (7)$$

and corresponds to a system of non-interacting thermal quasiparticles. The vacuum for thermal quasiparticles (hereafter denoted by $|0(T); \text{qp}\rangle$) is the thermal vacuum in the BCS approximation. The states $\beta_{jm}^\dagger |0(T); \text{qp}\rangle$

have positive excitation energies whereas the corresponding tilde-states $\tilde{\beta}_{jm}^\dagger|0(T); \text{qp}\rangle$ have negative energies.

The coefficients y_j^2 defined through (5) determine the average number of thermally excited Bogoliubov quasiparticles in the BCS thermal vacuum

$$\langle 0(T); \text{qp} | \alpha_{jm}^\dagger \alpha_{jm} | 0(T); \text{qp} \rangle = y_j^2 \quad (8)$$

and, thus, coincide with the thermal occupation factors of the Fermi-Dirac statistics. Since the thermal vacuum $|0(T); \text{qp}\rangle$ contains a certain number of Bogoliubov quasiparticles, excited states can be built on $|0(T); \text{qp}\rangle$ by either adding or removing a Bogoliubov quasiparticle. Because of

$$\begin{aligned} \alpha_{jm}^\dagger |0(T); \text{qp}\rangle &= x_j \beta_{jm}^\dagger |0(T); \text{qp}\rangle, \\ \alpha_{\bar{j}\bar{m}} |0(T); \text{qp}\rangle &= -iy_j \tilde{\beta}_{\bar{j}\bar{m}}^\dagger |0(T); \text{qp}\rangle \\ (\alpha_{\bar{j}\bar{m}} &= (-1)^{j-m} \alpha_{j-m}) \end{aligned} \quad (9)$$

the first process corresponds to the creation of a non-tilde thermal quasiparticle with positive energy, whereas the second process creates a tilde quasiparticle with negative energy.

In the next step of the approximate diagonalization of \mathcal{H}_{QPM} , long-range correlations due to the particle-hole interaction are taken into account within the proton-neutron TQRPA. The part of \mathcal{H}_{ph} in (2) responsible for charge-exchange excitations reads

$$\begin{aligned} \mathcal{H}_{\text{ph}}^{\text{ch}} &= -2 \sum_{\lambda\mu} \kappa_1^{(\lambda)} (M_{\lambda\mu}^\dagger M_{\lambda\mu} - \tilde{M}_{\lambda\mu}^\dagger \tilde{M}_{\lambda\mu}) \\ &\quad - 2 \sum_{L\lambda\mu} \kappa_1^{(L\lambda)} (S_{L\lambda\mu}^\dagger S_{L\lambda\mu} - \tilde{S}_{L\lambda\mu}^\dagger \tilde{S}_{L\lambda\mu}), \end{aligned} \quad (10)$$

where $M_{\lambda\mu}^\dagger$ and $S_{L\lambda\mu}^\dagger$ are single-particle multipole and spin-multipole operators:

$$\begin{aligned} M_{\lambda\mu}^\dagger &= \sum_{\substack{j_p m_p \\ j_n m_n}} \langle j_p m_p | i^\lambda r^\lambda Y_{\lambda\mu}(\theta, \phi) t^{(-)} | j_n m_n \rangle a_{j_p m_p}^\dagger a_{j_n m_n}, \\ S_{L\lambda\mu}^\dagger &= \sum_{\substack{j_p m_p \\ j_n m_n}} \langle j_p m_p | i^\lambda r^\lambda [Y_L \sigma]_\mu^\lambda t^{(-)} | j_n m_n \rangle a_{j_p m_p}^\dagger a_{j_n m_n}, \\ [Y_L \sigma]_\mu^\lambda &= \sum_{M, m} \langle LM 1m | \lambda\mu \rangle Y_{LM}(\theta, \phi) \sigma_m. \end{aligned} \quad (11)$$

The parameters $\kappa_1^{(\lambda)}$ and $\kappa_1^{(L\lambda)}$ denote the strength parameters of the isovector multipole and spin-multipole

forces, respectively. The states of natural parity are generated by the multipole and spin-multipole $L = \lambda$ interactions, while the spin-multipole interactions with $L = \lambda \pm 1$ are responsible for the states of unnatural parity.

Within the TFD formalism the TQRPA equations are derived in the following way. First, $\mathcal{H}_{\text{ph}}^{\text{ch}}$ is written in terms of the thermal quasiparticle operators. Then, the sum of (7) and $\mathcal{H}_{\text{ph}}^{\text{ch}}$ is diagonalized with respect to charge-exchange thermal phonons.

The thermal phonon creation operator $Q_{\lambda\mu i}^\dagger$ is defined as a linear superposition of the proton-neutron thermal two-quasiparticle operators

$$\begin{aligned} Q_{\lambda\mu i}^\dagger &= \sum_{j_p j_n} \left(\psi_{j_p j_n}^{\lambda i} [\beta_{j_p}^\dagger \beta_{j_n}^\dagger]_\mu^\lambda + \tilde{\psi}_{j_p j_n}^{\lambda i} [\tilde{\beta}_{j_p}^\dagger \tilde{\beta}_{j_n}^\dagger]_\mu^\lambda \right. \\ &\quad + i\eta_{j_p j_n}^{\lambda i} [\beta_{j_p}^\dagger \tilde{\beta}_{j_n}^\dagger]_\mu^\lambda + i\tilde{\eta}_{j_p j_n}^{\lambda i} [\tilde{\beta}_{j_p}^\dagger \beta_{j_n}^\dagger]_\mu^\lambda \\ &\quad + \phi_{j_p j_n}^{\lambda i} [\beta_{j_p} \beta_{j_n}]_\mu^\lambda + \tilde{\phi}_{j_p j_n}^{\lambda i} [\tilde{\beta}_{j_p} \tilde{\beta}_{j_n}]_\mu^\lambda \\ &\quad \left. + i\xi_{j_p j_n}^{\lambda i} [\beta_{j_p} \tilde{\beta}_{j_n}]_\mu^\lambda + i\tilde{\xi}_{j_p j_n}^{\lambda i} [\tilde{\beta}_{j_p} \beta_{j_n}]_\mu^\lambda \right), \end{aligned} \quad (12)$$

where $[\]_\mu^\lambda$ denotes the coupling of single-particle angular momenta j_n, j_p to total angular momentum λ . Now the thermal equilibrium state is treated as the vacuum $|0(T); \text{ph}\rangle$ for the thermal phonon annihilation operators.

The thermal phonon operators are assumed to commute as bosonic operators, i.e., $[Q_{\lambda\mu i}, Q_{\lambda'\mu' i'}^\dagger] = \delta_{\lambda\lambda'} \delta_{\mu\mu'} \delta_{ii'}$. This assumption imposes the following constraint on the phonon amplitudes:

$$\begin{aligned} \sum_{j_p j_n} \left(\psi_{j_p j_n}^{\lambda i} \psi_{j_p j_n}^{\lambda i'} + \tilde{\psi}_{j_p j_n}^{\lambda i} \tilde{\psi}_{j_p j_n}^{\lambda i'} + \eta_{j_p j_n}^{\lambda i} \eta_{j_p j_n}^{\lambda i'} \right. \\ \left. + \tilde{\eta}_{j_p j_n}^{\lambda i} \tilde{\eta}_{j_p j_n}^{\lambda i'} - \phi_{j_p j_n}^{\lambda i} \phi_{j_p j_n}^{\lambda i'} - \tilde{\phi}_{j_p j_n}^{\lambda i} \tilde{\phi}_{j_p j_n}^{\lambda i'} \right. \\ \left. - \xi_{j_p j_n}^{\lambda i} \xi_{j_p j_n}^{\lambda i'} - \tilde{\xi}_{j_p j_n}^{\lambda i} \tilde{\xi}_{j_p j_n}^{\lambda i'} \right) = \delta_{ii'}. \end{aligned} \quad (13)$$

Furthermore, the phonon amplitudes obey the closure relation.

Demanding that the vacuum of thermal phonons obeys the thermal state condition (1) and applying the variational principle to the average value of thermal Hamiltonian with respect to one-phonon states $Q_{\lambda\mu i}^\dagger|0(T); \text{ph}\rangle$ or $\tilde{Q}_{\lambda\mu i}^\dagger|0(T); \text{ph}\rangle$ [48] under the constraints (13) one gets a system of linear equations for the amplitudes $\psi_{j_p j_n}^{\lambda i}$, $\tilde{\psi}_{j_p j_n}^{\lambda i}$, $\eta_{j_p j_n}^{\lambda i}$, $\tilde{\eta}_{j_p j_n}^{\lambda i}$, etc. The system has a nontrivial solution if the energy $\omega_{\lambda i}$ of the thermal one-phonon state obeys the following secular equation:

$$\begin{vmatrix} X_{aa}^{(+)} - \frac{1}{\kappa_1^{(a)}} & X_{aa}^{(+ -)} & X_{ab}^{(+)} & X_{ab}^{(+ -)} \\ X_{aa}^{(- +)} & X_{aa}^{(-)} - \frac{1}{\kappa_1^{(a)}} & X_{ab}^{(- +)} & X_{ab}^{(-)} \\ X_{ab}^{(+)} & X_{ab}^{(+ -)} & X_{bb}^{(+)} - \frac{1}{\kappa_1^{(b)}} & X_{bb}^{(+ -)} \\ X_{ab}^{(- +)} & X_{ab}^{(-)} & X_{ab}^{(- +)} & X_{bb}^{(-)} - \frac{1}{\kappa_1^{(b)}} \end{vmatrix} = 0, \quad (14)$$

where $a \equiv \lambda$ and $b \equiv \lambda\lambda$ for excitations of natural parity, while $a \equiv (\lambda - 1)\lambda$ and $b \equiv (\lambda + 1)\lambda$ for unnatural parity excitations. The functions $X_{cd}^{(\pm)}$, $X_{cd}^{(\pm\mp)}$ ($c = a, b$ and $d = a, b$) in (14) are defined as

$$\begin{aligned} X_{cd}^{(\pm)}(\omega) &= \frac{2}{\hat{\lambda}^2} \sum_{j_p j_n} f_{j_p j_n}^{(c)} f_{j_p j_n}^{(d)} \left\{ \frac{\varepsilon_{j_p j_n}^{(+)} (u_{j_p j_n}^{(\pm)})^2}{(\varepsilon_{j_p j_n}^{(+)} - \omega)^2} \right. \\ &\quad \left. \times (1 - y_{j_p}^2 - y_{j_n}^2) - \frac{\varepsilon_{j_p j_n}^{(-)} (v_{j_p j_n}^{(\mp)})^2}{(\varepsilon_{j_p j_n}^{(-)} - \omega)^2} (y_{j_p}^2 - y_{j_n}^2) \right\}, \\ X_{cd}^{(\pm\mp)}(\omega) &= \frac{2\omega}{\hat{\lambda}^2} \sum_{j_p j_n} f_{j_p j_n}^{(c)} f_{j_p j_n}^{(d)} \left\{ \frac{u_{j_p j_n}^{(\pm)} u_{j_p j_n}^{(\mp)}}{(\varepsilon_{j_p j_n}^{(+)} - \omega)^2} \right. \\ &\quad \left. \times (1 - y_{j_p}^2 - y_{j_n}^2) - \frac{v_{j_p j_n}^{(\pm)} v_{j_p j_n}^{(\mp)}}{(\varepsilon_{j_p j_n}^{(-)} - \omega)^2} (y_{j_p}^2 - y_{j_n}^2) \right\}. \quad (15) \end{aligned}$$

Here $f_{j_p j_n}^{(\lambda)}$ and $f_{j_p j_n}^{(\lambda L)}$ denote the reduced single-particle matrix elements of the multipole and spin-multipole operators (11); $u_{j_p j_n}^{(\pm)} = u_{j_p} v_{j_n} \pm v_{j_p} u_{j_n}$ and $v_{j_p j_n}^{(\pm)} = u_{j_p} u_{j_n} \pm v_{j_p} v_{j_n}$; $\varepsilon_{j_p j_n}^{(\pm)} = \varepsilon_{j_p} \pm \varepsilon_{j_n}$; $\hat{\lambda} = \sqrt{2\lambda + 1}$.

Let us consider the secular equation in detail. The poles $\varepsilon_{j_p j_n}^{(-)}$ which do not exist in the QRPA equations at zero temperature arise from the crossed terms $\beta^\dagger \tilde{\beta}^\dagger$ in the thermal phonon operator definition (12). Due to these poles, new states appear in a low-energy part of the thermal excitation spectrum. In contrast to the zero temperature case, the negative solutions of the secular equation now have a physical meaning. They correspond to the tilde thermal one-phonon states and arise from $\tilde{\beta}^\dagger \tilde{\beta}^\dagger$ terms in the thermal phonon operator. As it was noted above, creation of a tilde thermal quasiparticle corresponds to the annihilation of a thermally excited Bogoliubov quasiparticle. Consequently, excitations of low- and negative-energy thermal phonons correspond to transitions from thermally excited nuclear states. Furthermore, when the pairing correlations vanish (i.e., $T > T_{\text{cr}}$), some poles no longer contribute to the secular equation since the corresponding numerators vanish. This is true for particle-particle and hole-hole $\varepsilon_{j_p j_n}^{(+)}$ poles as well as for particle-hole $\varepsilon_{j_p j_n}^{(-)}$ poles.

The expressions for the thermal charge-exchange phonon amplitudes can be found in [28]. The amplitudes depend on both the quasiparticle and the phonon thermal occupation numbers. Some remarks are in order. TQRPA equations for GT excitations at finite temperature were also derived in [34]. They were obtained using the equation of motion method by replacing vacuum expectation values by thermal averages, i.e., without applying the TFD formalism and doubling the Hilbert space. Therefore, in contrast with the present study negative solutions of the TQRPA equations were neglected in [34].

After diagonalization within the TQRPA the thermal Hamiltonian \mathcal{H}_{QPM} becomes

$$\mathcal{H}_{\text{QPM}} = \sum_{\lambda\mu i} \omega_{\lambda i} (Q_{\lambda\mu i}^\dagger Q_{\lambda\mu i} - \tilde{Q}_{\lambda\mu i}^\dagger \tilde{Q}_{\lambda\mu i}). \quad (16)$$

The vacuum $|0(T); \text{ph}\rangle$ of thermal phonons is the thermal vacuum in the thermal quasiparticle RPA. Since we use the thermal BCS approximation, which violates the particle number, the charge-exchange thermal one-phonon states are superpositions of states, which belong to the daughter nuclei $(N - 1, Z + 1)$ and $(N + 1, Z - 1)$. They decouple at temperatures $T \geq T_{\text{cr}}$, when the pairing correlations vanish. Then, if the state $Q_{\lambda\mu i}^\dagger |0(T); \text{ph}\rangle$ belongs to the $(N \pm 1, Z \mp 1)$ nucleus, the state $\tilde{Q}_{\lambda\mu i}^\dagger |0(T); \text{ph}\rangle$ is in the $(N \mp 1, Z \pm 1)$ nucleus.

III. ELECTRON CAPTURE RATES

Considering electron capture in stellar environments we make the following assumptions: 1. the temperature in the stellar interior is so high that atoms are fully ionized, and the surrounding electron gas is described by a Fermi-Dirac distribution, with temperature T and chemical potential μ_e . Neutrinos escape freely from the interior of the star. Hence no Pauli blocking for neutrinos is considered in the final state. 2. the parent nucleus is in a thermal equilibrium state treated as the thermal (phonon) vacuum. 3. electron capture leads to charge-exchange transitions from the thermal vacuum to thermal one-phonon states.

Under these circumstances the electron capture rate is the sum of the transition rates from the thermal vacuum

to the i -th thermal one-phonon state of the multipolarity J

$$\lambda^{\text{ec}} = \frac{\ln 2}{6150 \text{ sec}} \sum_J \sum_i \Phi_{Ji}^{(+)} F_i^{\text{ec}} = \sum_J \sum_i \lambda_{Ji}^{\text{ec}}. \quad (17)$$

Here $\Phi_{Ji}^{(+)}$ is the squared reduced matrix element of the transition operator between the thermal phonon vacuum and a thermal one-phonon state (see below); F_i^{ec} is a phase space factor which depends on the transition energy $E_{Ji}^{(+)}$ and can be found elsewhere [9].

Denoting the proton-to-neutron ($p \rightarrow n$) transition operator with multipolarity J as $D_J^{(+)}$ one obtains the following expression for the transition strength $\Phi_{Ji}^{(+)}$

$$\begin{aligned} \Phi_{Ji}^{(+)} &= \left| \langle 0(T); \text{ph} \| Q_{JM_i} D_J^{(+)} \| 0(T); \text{ph} \rangle \right|^2 \\ &= \left(\sum_{j_p j_n} (-1)^{j_n - j_p + J} d_J^{(+)}(j_p j_n) \Omega(j_p j_n; Ji) \right)^2, \end{aligned} \quad (18)$$

where $d_J^{(+)}(j_p j_n) = \langle j_n \| D_J^{(+)} \| j_p \rangle$ is a reduced single-particle matrix element of the transition operator, and the function $\Omega(j_p j_n; Ji)$ is given by

$$\begin{aligned} \Omega(j_p j_n; Ji) &= v_{j_p} u_{j_n} (x_{j_p} x_{j_n} \psi_{j_p j_n}^{Ji} + y_{j_p} y_{j_n} \tilde{\phi}_{j_p j_n}^{Ji}) \\ &\quad + u_{j_p} v_{j_n} (y_{j_p} y_{j_n} \tilde{\psi}_{j_p j_n}^{Ji} + x_{j_p} x_{j_n} \phi_{j_p j_n}^{Ji}) \\ &\quad - v_{j_p} v_{j_n} (x_{j_p} y_{j_n} \eta_{j_p j_n}^{Ji} + y_{j_p} x_{j_n} \tilde{\xi}_{j_p j_n}^{Ji}) \\ &\quad + u_{j_p} u_{j_n} (y_{j_p} x_{j_n} \tilde{\eta}_{j_p j_n}^{Ji} + x_{j_p} y_{j_n} \xi_{j_p j_n}^{Ji}). \end{aligned} \quad (19)$$

The transition strength to the tilde one-phonon state can be easily obtained from (18) and (19) by changing non-tilde phonon amplitudes by their tilde counterparts and vice versa. (The expressions for the transition strengths $\Phi_{Ji}^{(-)}$ corresponding to inverse $n \rightarrow p$ transitions are given in [28]. It has been proved in [28] that the approach used here fulfills the Ikeda sum rule for Fermi and Gamow-Teller transitions.)

The transition energy (parent excitation energy) $E_{Ji}^{(+)}$ can be obtained from the energy shift between the proton subsystem of the parent nucleus and the neutron subsystem of the daughter nucleus including the proton-neutron mass difference. Thus we have

$$E_{Ji}^{(+)} = \omega_{Ji} + (\Delta\mu_{np} + \Delta m_{np}), \quad (20)$$

where $\Delta\mu_{np} = \mu_p - \mu_n$ is the difference between neutron and proton chemical potentials and $\Delta m_{np} = m_n - m_p$ is the neutron-proton mass splitting. Note, that at finite temperature the energies $E_{Ji}^{(+)}$ as well as ω_{Ji} can be both positive and negative. Thus, to the capture process thermal one-phonon states with both positive and negative values of $E_{Ji}^{(+)}$ contribute to the rate.

In what follows in (17) we take into account the contributions from allowed (Gamow-Teller and Fermi) transitions and first-forbidden transitions. The operators of

allowed Fermi and Gamow-Teller transitions are taken in the standard form

$$D_{0+}^{(+)} = g_V t^{(+)}, \quad D_{1+}^{(+)} = g_A \boldsymbol{\sigma} t^{(+)}, \quad (21)$$

where $t^{(+)}$ is the isospin raising operator. For the operators of the first-forbidden $n \rightarrow p$ transitions the non-relativistic form is used

$$\begin{aligned} D_{0-}^{(+)} &= g_A \left[\frac{\boldsymbol{\sigma} \cdot \mathbf{p}}{m} + \frac{\alpha Z}{2R} i \boldsymbol{\sigma} \cdot \mathbf{r} \right] t^{(+)}, \\ D_{1-}^{(+)} &= \left[g_V \frac{\mathbf{p}}{m} - \frac{\alpha Z}{2R} (g_A \boldsymbol{\sigma} \times \mathbf{r} - i g_V \mathbf{r}) \right] t^{(+)}, \\ D_{2-}^{(+)} &= i \frac{g_A}{\sqrt{3}} [\boldsymbol{\sigma} \cdot \mathbf{r}]_{\mu}^2 \sqrt{p_e^2 + q_{\nu}^2} t^{(+)}. \end{aligned} \quad (22)$$

In Eqs. (21) and (22) \mathbf{r} , \mathbf{p} , and $\boldsymbol{\sigma}$ refer to the coordinate, momentum and spin operators of a nucleon, $g_V = 1$ and $g_A = -1.25$ denote the vector and axial coupling constants, α is the fine structure constant, Z , R are the charge and the radius of the nucleus; m is the nucleon mass and p_e and q_{ν} denote the momenta of the incoming electron and outgoing neutrino, respectively.

IV. IRON ISOTOPES

In this section we discuss the numerical results for the pf -shell nuclei $^{54,56}\text{Fe}$. Experimental data are available for these nuclei to test our calculations at zero temperature. Moreover, these iron isotopes are among the most essential nuclei in their importance for the electron capture process for the early presupernova collapse [6, 35].

The proton and neutron mean fields are described by spherically symmetric Woods-Saxon potentials with parameters from [36]. We only readjust the potential depths to fit the proton and neutron binding energies of the parent nucleus to their experimental values. The single-particle basis includes all discrete bound states as well as selected quasi-bound states with large j in the continuum. The proton (neutron) pairing strength parameters $G_{p(n)}$ are fixed to reproduce the odd-even mass difference through a four term formula [37] involving the experimental binding energies [38]. At $T = 0$ the obtained proton and neutron BCS energy gaps are: $\Delta_{p(n)} = 1.52$ (0.0) MeV for ^{54}Fe , [49] $\Delta_{p(n)} = 1.57$ (1.36) MeV for ^{56}Fe . The isovector strength parameters $\kappa_1^{(01)}$ and $\kappa_1^{(21)}$ are adjusted to reproduce the experimental centroid energies of the GT_- and GT_+ resonances in the nuclei under consideration [39, 40, 41]. The corresponding values of $\kappa_1^{(01)}$ and $k_1^{(21)}$ are in agreement with the rough estimates in [42]. The spin-quadrupole interaction weakly affects the GT strength distributions.

The total GT strengths calculated with the bare GT_{\pm} operators $\sigma t^{(\pm)}$ are $S_+ = 6.6$, $S_- = 12.7$ in ^{54}Fe and $S_+ = 5.1$, $S_- = 17.0$ in ^{56}Fe respectively. These S_{\mp} values obey the Ikeda sum rule (a small deviation is

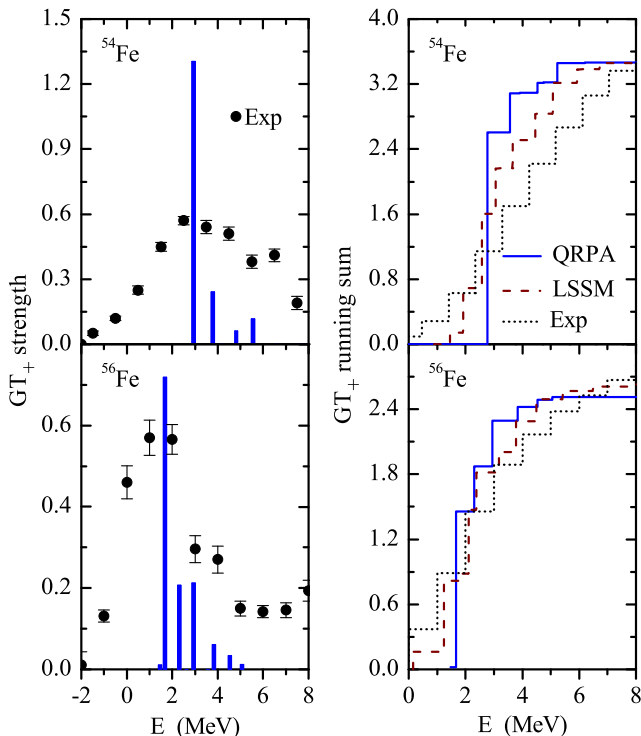


FIG. 1: (Color online) Left panels: Comparison of GT_+ experimental data [40, 41] with the calculated QRPA strength distributions for $^{54,56}\text{Fe}$. The QRPA peaks are scaled by 0.5 for convenience. Right panels: Comparison of the GT_+ running sums corresponding to the experimental, QRPA, and LSSM [9] strength distributions.

due to the incompleteness of our single particle basis) but noticeably overestimate experimental data (see e.g. [39, 40, 41]). This is common for any RPA (or QRPA) calculation of the GT strength and is remedied by an effective value for the axial weak coupling constant. We use $g_A^* = 0.74g_A$ as in shell-model calculations [9].

In Fig.1, the experimental and theoretical (quenched) distributions of GT_+ strengths are presented. Here we also compare the GT_+ running sums corresponding to the experimental, QRPA, and large scale shell-model (LSSM) [9] strength distributions. One can see that the QRPA calculations reproduce the resonance positions but not the fragmentation of the strength. It is a well known fact that RPA calculations cannot describe the full resonance width (at least in spherical nuclei) and produce only a part of it, the so-called Landau width. The latter is quite small for the GT resonance. As a result, the near threshold part of the GT_+ strength, which corresponds to transitions to low-lying 1^+ states in the daughter nuclei $^{54,56}\text{Mn}$, is not reproduced in our calculations. In this respect the shell-model calculations are clearly at an advantage.

We now turn to the temperature evolution of the GT_+ strength distributions. The strength distributions for $^{54,56}\text{Fe}$ at several temperatures are shown in Fig. 2. All

figures are plotted as a function of the energy transfer E to the parent nucleus.

With increasing temperature, in our model, two effects occur that influence the GT_+ strength distribution:

(i) At low temperatures, due to pairing, GT_+ transitions involve the breaking of a proton Cooper pair associated with some energy cost. This extra energy is removed at $T > T_{\text{cr}}$ ($T_{\text{cr}} \approx 0.8$ MeV) and the peak in the GT_+ distribution moves to smaller energies. Some extra energy has to be paid at low temperatures to add one more nucleon to the neutron subsystem of ^{56}Fe because of a non-zero neutron energy gap. Obviously, this energy is also removed at $T > T_{\text{cr}}$.

(ii) GT_+ transitions, which are Pauli blocked at low temperatures due to closed neutron subshells (e.g., $1f_{7/2}$ orbital), become thermally unblocked with increasing temperature. Similarly, protons which are thermally excited to higher orbitals can undergo GT_+ transitions. In TFD such transitions are taken into account by $\beta_{j_p}^{\dagger} \tilde{\beta}_{j_n}^{\dagger}$, $\tilde{\beta}_{j_p}^{\dagger} \beta_{j_n}^{\dagger}$, and $\tilde{\beta}_{j_p}^{\dagger} \tilde{\beta}_{j_n}^{\dagger}$ components of the thermal phonon. Because of thermally unblocked transitions, some GT_+ strength appears well below the zero-temperature threshold, including negative energies.

Due to the vanishing of the pairing correlations and appearance of negative- and low-energy transitions, the centroids of the GT_+ strength distributions in $^{54,56}\text{Fe}$ are shifted to lower excitation energies at high temperatures. Our calculations indicate that a temperature increase to 0.8 MeV results in the GT_+ centroid shifts of the order of 1.5 MeV for ^{54}Fe and 2.5 MeV for ^{56}Fe . Thus the present approach violates Brink's hypothesis. Similar results have been obtained in SMMC calculations of the GT centroids at finite temperatures. We also observe (see Fig. 2) a gradual decrease of the total GT_+ strength when the temperature increases from zero to 0.8 MeV. Nevertheless, as was pointed out above, the present approach preserves the Ikeda sum rule at finite temperatures.

The calculated GT_+ strength distributions have been used to obtain the stellar electron capture rates for $^{54,56}\text{Fe}$. The rates have been calculated for densities between $\log(\rho Y_e) = 7$ and $\log(\rho Y_e) = 10$ as a function of temperature T_9 ($T_9 = 10^9$ K and $1 \text{ MeV} \approx 11.6 T_9$). The comparison between the TQRPA rates and the large-scale shell-model results [10] is presented in Fig. 3.

As it must be, the electron capture rates increase with temperature and density. Due to the larger value of the zero-temperature threshold Q for ^{56}Fe , both approaches yield a higher rate for ^{54}Fe than for ^{56}Fe at a given temperature and density. Both approaches give very similar values for the strength and the location of the GT_+ resonance in $^{54,56}\text{Fe}$ at $T = 0$. Therefore, the excellent agreement between the TQRPA and shell model rates at $\log(\rho Y_e) = 10$ and low temperatures ($\mu_e \approx 11 \text{ MeV}$) is not surprising, since the rates are dominated by the resonance contribution.

The more interesting point is that at high temperatures

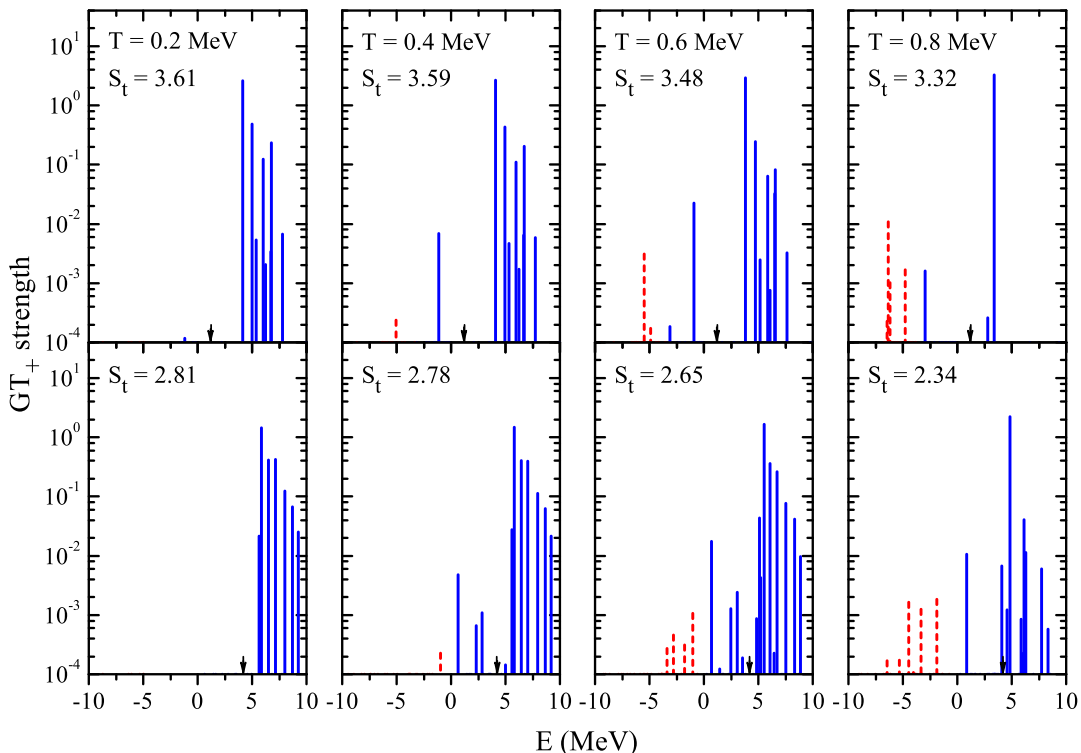


FIG. 2: (Color online) Temperature evolution of GT_+ strength distributions for ^{54}Fe (upper panels) and for ^{56}Fe (lower panels) versus parent excitation energy. The full (dashed) lines refer to transitions to non-tilde (tilde) thermal one-phonon states. S_t is the total GT_+ strength. The arrows indicate the zero-temperature threshold $Q = M_f - M_i$, where $M_{i,f}$ are the masses of the parent and daughter nuclei. $Q(^{54}\text{Fe}) = 1.21$ MeV and $Q(^{56}\text{Fe}) = 4.20$ MeV.

the TQRPA rates always surpass the shell-model ones. To understand this point, it needs to be clarified which part of the TQRPA GT_+ strength dominates the electron capture at a given temperature and density. To this end we calculate the relative contributions $\lambda_i^{\text{ec}}/\lambda^{\text{ec}}$ of different thermal one-phonon states to the capture rates for selected values of temperature and density, $(T_9, \log(\rho Y_e))$. The results are depicted in Fig. 4.

At low temperatures and densities (Fig. 4(a),(b)), i.e., when μ_e is small and high-energy electrons from the tail of the Fermi-Dirac distribution are not sufficiently available to allow for efficient capture on the GT_+ resonance, the TQRPA capture rates are dominated either by the negative-energy (^{54}Fe) or by the low-energy (^{56}Fe) part of the GT_+ strength which originates from thermally unblocked $p \rightarrow n$ transitions. The TQRPA rates are larger than those of the shell-model at low (T, ρ) due to differences in the strength and the energy of such transitions. We note that in the shell model evaluation negative-energy transitions were mainly included by back-resonances; i.e. by inverting the Fermi and GT_- strength distribution of ^{54}Mn and ^{56}Mn , respectively. Different to the TQRPA approach the shell model GT_- distributions of these nuclei are highly fragmented due to

correlations and have centroids at rather high excitation energies in ^{54}Fe and ^{56}Fe which, at low temperatures, are strongly suppressed by the Boltzmann factor. In particular, the differences in energy positions of the transitions are important since at low (T, ρ) the rates can change drastically by a small change in a transition energy. To see whether the TQRPA reliably predicts the energy and the strength of negative- and low-energy transitions one needs to go beyond the TQRPA.

At $\log(\rho Y_e) = 9$ and $T_9 < 5$ ($\mu_e \approx 5.1$ MeV) the near threshold part of the GT_+ strength dominates the capture rates. Since this part is not reproduced within the TQRPA, the rates appear to be smaller than the LSSM ones. To test this hypothesis, the capture rates at $\log(\rho Y_e) = 9$ have been calculated – guided by the shell-model GT_+ distributions [9] – assuming that the near threshold GT_+ strengths for ^{54}Fe and ^{56}Fe are 0.1 and 0.2, respectively. We therefore assign the value 0.1 (0.2) to the GT_+ strength in ^{54}Fe (^{56}Fe) at the zero-temperature threshold. (A similar method was used in [5, 6] to include the contribution of low-lying transitions.) This yields a much better agreement between the TQRPA and shell-model rates (see Fig. 3). Thus, to improve the reliability of the TQRPA for the cal-

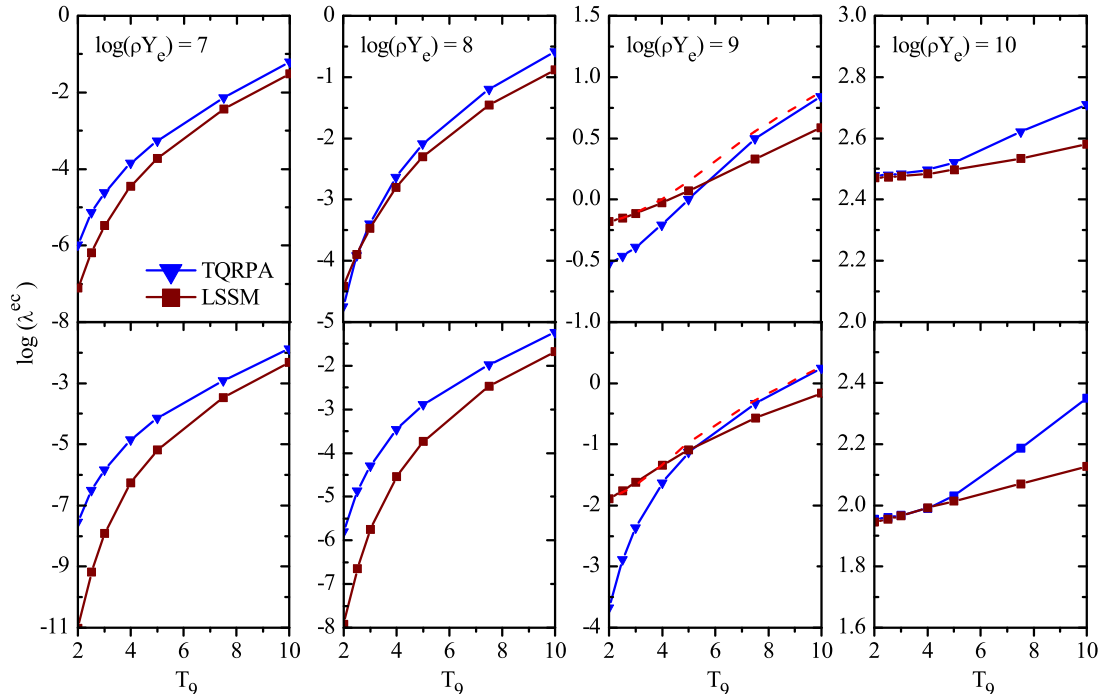


FIG. 3: (Color online) Electron capture rates for ^{54}Fe (upper panels) and ^{56}Fe (lower panels) calculated using the TQRPA approach as a function of temperature (T_9 measures the temperature in 10^9 K) and for selected values of density ρY_e (in g cm^{-3}). For comparison, the LSSM rates [10] are also shown. The dashed lines at $\log(\rho Y_e) = 9$ correspond to the TQRPA rates calculated with the assigned near threshold strength (see text).

calculation of stellar electron capture rates at intermediate densities and low temperatures, the fragmentation of the GT_+ resonance should be considered to reproduce the near threshold GT_+ strength. At higher temperatures the near threshold strength becomes less important. In Fig. 4(c),(d) the relative contributions $\lambda_i^{\text{ec}}/\lambda^{\text{ec}}$ at $(T_9, \log(\rho Y_e)) = (5, 9)$ with and without the assigned near threshold strength are depicted. As can be seen, the contribution from the near threshold strength is not dominant.

When the temperature approaches $T_9 \approx 10$, the rates are dominated by the strong transitions involving the GT_+ resonance at low (Fig. 4(e)) as well as at high (Fig. 4(f)) densities. (Note that at $\log(\rho Y_e) = 7$ and high temperatures the contribution of negative-energy transitions is non-negligible.) As was discussed above, the TQRPA predicts that with increasing temperature the GT_+ resonance shifts to lower excitation energies. This explains why the TQRPA rates always surpass the LSSM ones at high temperatures.

Thus, only at high densities and low temperatures the TQRPA and LSSM electron capture rates for $^{54,56}\text{Fe}$ are in a good agreement. As was mentioned above the disagreement at moderate densities and low temperatures can be removed by considering the fragmentation of the GT_+ strength. For a separable residual interaction used here this can be done following the method developed

within the quasiparticle-phonon nuclear model, i.e., by taking into account the phonon coupling. The interesting question is how the phonon coupling affects the negative- and low-energy part of the GT_+ strength, which dominates the capture rate at low temperatures and densities. This is an open question and requires further investigations.

V. NEUTRON-RICH GERMANIUM ISOTOPES

During gravitational collapse the nuclear composition moves towards higher mass number and more neutron-rich nuclei. Eventually nuclei will have all neutron pf -shell orbits filled, with valence neutrons in the sdg -shell ($N > 40$) and valence protons within the pf -shell ($Z < 40$). The Pauli principle blocks GT_+ transitions in such neutron-rich nuclei if the independent particle model is used. It has been demonstrated in [4] that at high enough temperatures, $T \sim 1.5$ MeV, GT_+ transitions become unblocked by thermal excitations which either move protons into the $1g_{9/2}$ orbital or remove neutrons from the pf -shell. An alternative unblocking mechanism, configuration mixing induced by the residual interaction, was considered in [20]. Based on this approach it was found that electron capture on nuclei with $N > 40$ is also dominated by GT_+ transitions even at rather low

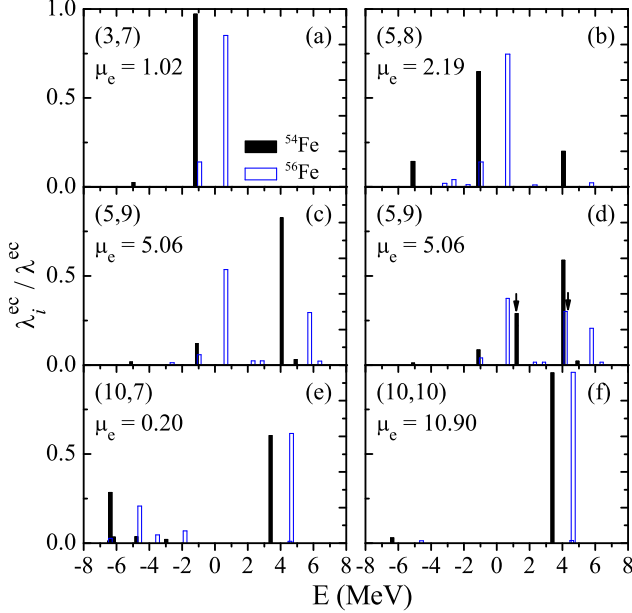


FIG. 4: (Color online) Relative contribution $\lambda_i^{ec}/\lambda^{ec}$ of i -th thermal one-phonon state to the electron capture rate on $^{54,56}\text{Fe}$ for selected values of temperature and density, $(T_9, \log(\rho Y_e))$. The electron chemical potential μ_e is in units of MeV; E is the transition energy to i -th thermal one-phonon state. The arrows in panel (d) indicate the relative contributions of the assigned near threshold strengths (see text).

stellar temperatures, $T \sim 0.5$ MeV. Contrary to [4], it was argued that unblocking effects due to mixing are not too sensitive to increasing temperature.

Consistent calculations of the electron capture rates for neutron-rich nuclei are not yet feasible in the shell model due to the large model space. In [20] the capture rates have been calculated adopting a hybrid model: The partial occupation numbers calculated within the SMMC approach at finite temperature were used in calculations based on the RPA. In this subsection, using the germanium isotopes $^{76,78,80}\text{Ge}$ as examples, we apply the TQRPA formalism to calculate electron capture rates on neutron-rich nuclei. Particular attention is paid to the temperature dependence of the unblocking effect.

For our TQRPA calculations the parameters of the model Hamiltonian for $^{76,78,80}\text{Ge}$ are chosen in the same manner as for $^{54,56}\text{Fe}$. The sequence of single-particle levels obtained is close to that used in [4] for ^{82}Ge . For pairing gaps we obtain: $\Delta_{p(n)} = 1.50$ (1.57) MeV for ^{76}Ge , $\Delta_{p(n)} = 1.59$ (1.42) MeV for ^{78}Ge , and $\Delta_{p(n)} = 1.39$ (1.35) MeV for ^{80}Ge . Our calculations take into account both the allowed (GT and Fermi) and first-forbidden transitions with $J \leq 2$. To generate one-phonon states of natural and unnatural parity we use the isovector multipole and spin-multipole strength parameters $\kappa_1^{(\lambda)}$, $\kappa_1^{(L\lambda)}$ ($\lambda = 0, 1, 2$) according to [42, 43]

As a representative example, the strength distribution

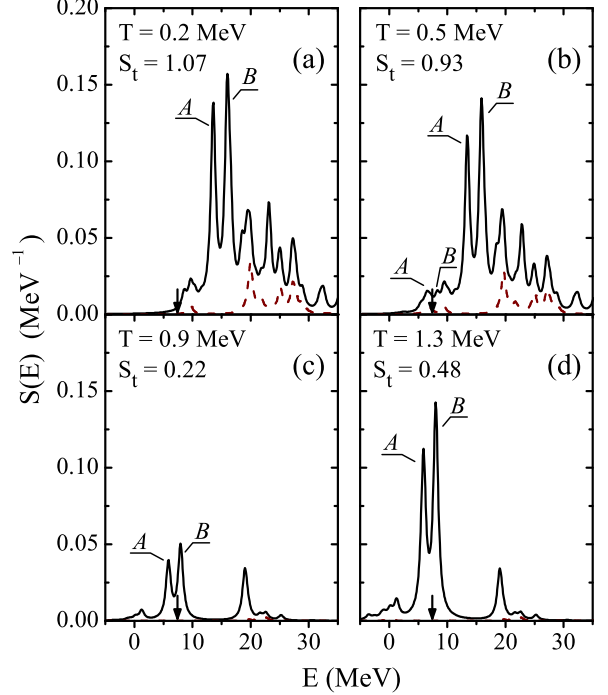


FIG. 5: (Color online) Strength distribution (folded) of allowed (0^+ and 1^+) $p \rightarrow n$ transitions in ^{76}Ge at various temperatures T . E denotes the transition energy. The contribution of 0^+ transitions is shown by the dashed line. S_t is the total strength. The arrows indicate the zero temperature threshold $Q(^{76}\text{Ge}) = M_f - M_i = 7.52$ MeV. The letters label the transitions: $A \equiv 1f_{7/2}^p \rightarrow 1f_{5/2}^n$, $B \equiv 1g_{9/2}^p \rightarrow 1g_{7/2}^n$.

of allowed $p \rightarrow n$ transitions from ^{76}Ge for different values of temperature is displayed in Fig. 5. The distributions have been folded with a Breit-Wigner function of 1 MeV width. As it follows from our study as well as from [4, 20], two single-particle transitions mainly contribute to the total GT_+ strength in neutron-rich germanium isotopes. These are the $1g_{9/2}^p \rightarrow 1g_{7/2}^n$ particle-particle and $1f_{7/2}^p \rightarrow 1f_{5/2}^n$ hole-hole transitions. In an independent particle model both transitions are blocked at zero temperature. However, in the present model they become unblocked due to pairing correlations and thermal excitations. Referring to Fig. 5 it is observed that, with increasing temperature, the peaks in the GT_+ distribution shift to lower excitation energies and the total strength decreases in the vicinity of the critical temperature ($T_{\text{cr}} \sim 0.8$ MeV)[50]. The shift is of the order of 8 MeV and, hence, cannot be explained solely by removing the extra energy needed to break a proton pair.

To explain both effects we neglect the residual particle-hole interaction and consider the pairing interaction only. (As it follows from our study, the position of the GT_+ peaks in $^{76,78,80}\text{Ge}$ is little affected by the inclusion of QRPA correlations and thermal one-phonon states can be considered as thermal two-quasiparticle states.) At fi-

nite temperature the GT_+ operator can excite configurations of four different types, namely, $[\beta_{j_p}^\dagger \beta_{j_n}^\dagger]_{\mu}^1$, $[\tilde{\beta}_{j_p}^\dagger \tilde{\beta}_{j_n}^\dagger]_{\mu}^1$, $[\tilde{\beta}_{j_p}^\dagger \beta_{j_n}^\dagger]_{\mu}^1$, and $[\beta_{j_p}^\dagger \tilde{\beta}_{j_n}^\dagger]_{\mu}^1$. The respective transition energies and transition strengths are

$$\begin{aligned}
E_1(j_p \rightarrow j_n) &= \varepsilon_{j_p} + \varepsilon_{j_n} + Q^*, \\
\Phi_1(j_p \rightarrow j_n) &= (f_{j_p j_n}^1)^2 v_{j_p}^2 u_{j_n}^2 x_{j_p}^2 x_{j_n}^2; \\
E_2(j_p \rightarrow j_n) &= -(\varepsilon_{j_p} + \varepsilon_{j_n}) + Q^*, \\
\Phi_2(j_p \rightarrow j_n) &= (f_{j_p j_n}^1)^2 u_{j_p}^2 v_{j_n}^2 y_{j_p}^2 y_{j_n}^2; \\
E_3(j_p \rightarrow j_n) &= \varepsilon_{j_p} - \varepsilon_{j_n} + Q^*, \\
\Phi_3(j_p \rightarrow j_n) &= (f_{j_p j_n}^1)^2 v_{j_p}^2 v_{j_n}^2 x_{j_p}^2 y_{j_n}^2; \\
E_4(j_p \rightarrow j_n) &= -(\varepsilon_{j_p} - \varepsilon_{j_n}) + Q^*, \\
\Phi_4(j_p \rightarrow j_n) &= (f_{j_p j_n}^1)^2 u_{j_p}^2 u_{j_n}^2 y_{j_p}^2 x_{j_n}^2, \quad (23)
\end{aligned}$$

where $Q^* = \Delta\mu_{np} + \Delta m_{np}$ (see Eq. (20)). In the following $j_p \rightarrow j_n$ refer either to the $1g_{9/2}^p \rightarrow 1g_{7/2}^n$ or the $1f_{7/2}^p \rightarrow 1f_{5/2}^n$ transition.

At $T < T_{cr}$ the excitation of the $[\beta_{j_p}^\dagger \beta_{j_n}^\dagger]_{\mu}^1$ configuration dominates the strength distribution because of the factor $x_{j_p}^2 x_{j_n}^2 \sim 1$ in $\Phi_1(j_p \rightarrow j_n)$. Therefore, at relatively low temperatures, when configuration mixing induced by pairing correlations in the ground state is the main unblocking mechanism, the position of the GT_+ peaks is given by $E_1(1g_{9/2}^p \rightarrow 1g_{7/2}^n)$ and $E_1(1f_{7/2}^p \rightarrow 1f_{5/2}^n)$ (Fig. 5(a),(b)). With increasing temperature states having internal configurations other than those of the nuclear ground state gain statistical weight and, in particular, the pairing correlations in these excited states decrease. When the pairing correlations disappear and the factors $v_{j_p}^2 u_{j_n}^2$ in $\Phi_1(j_p \rightarrow j_n)$ become zero, the peaks considered completely vanish (Fig. 5(c)). The value of $\Phi_2(j_p \rightarrow j_n)$ becomes zero as well. At $T \geq T_{cr}$ the poles $\varepsilon_{1g_{9/2}^p} + \varepsilon_{1g_{7/2}^n}$ and $\varepsilon_{1f_{7/2}^p} + \varepsilon_{1f_{5/2}^n}$ no longer contribute to the secular equation (14).

At $T > T_{cr}$ GT_+ transitions from (to) thermally occupied (unblocked) orbitals dominate the strength distribution. Such transitions correspond to the excitation of the $[\tilde{\beta}_{1g_{9/2}^p}^\dagger \beta_{1g_{7/2}^n}^\dagger]_{\mu}^1$ and $[\beta_{1f_{7/2}^p}^\dagger \tilde{\beta}_{1f_{5/2}^n}^\dagger]_{\mu}^1$ configurations and their energies are $E_4(1g_{9/2}^p \rightarrow 1g_{7/2}^n)$ and $E_3(1f_{7/2}^p \rightarrow 1f_{5/2}^n)$, respectively. Neglecting Δm_{np} , these energies are the energy difference between the final and initial single-particle states, i.e., $E_4(1g_{9/2}^p \rightarrow 1g_{7/2}^n) \approx E_{1g_{7/2}^n} - E_{1g_{9/2}^p}$ and $E_3(1f_{7/2}^p \rightarrow 1f_{5/2}^n) \approx E_{1f_{5/2}^n} - E_{1f_{7/2}^p}$. Because of the thermally unblocked transitions the GT_+ peaks appear near the zero temperature threshold (Fig. 5(d)).

Thus, in contrast to [20], we find that the unblocking effect for GT_+ transitions in neutron-rich nuclei is sensitive to increasing temperature. No shift to lower excitation energies for the GT_+ peaks or decrease of the total GT_+ strength in the vicinity of the critical temperature were observed in [20]. To understand these differences we compare again the approximations underlying

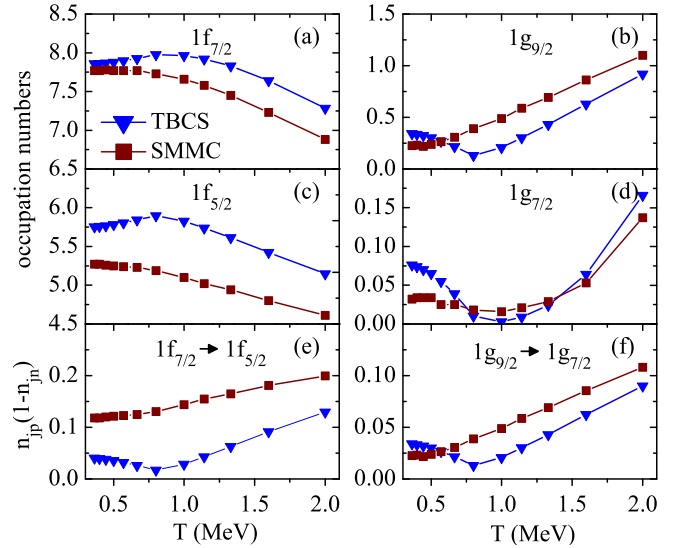


FIG. 6: (Color online) Upper panels: Occupation numbers for the $1f_{7/2}$, $1g_{9/2}$ proton orbitals in ^{76}Ge as a function of temperature. Middle panels: Occupation numbers for the $1f_{5/2}$, $1g_{7/2}$ neutron orbitals. Lower panels: The unblocking probabilities for the $1f_{7/2}^p \rightarrow 1f_{5/2}^n$ and $1g_{9/2}^p \rightarrow 1g_{7/2}^n$ transitions.

the present model and the hybrid approach of [20]. The TQRPA has the virtue of consistency. It describes correlations by configuration mixing derived from a pairing interaction up to the $2p2h$ level. In the hybrid model occupation numbers at finite temperature are calculated within the SMMC approach, accounting for all many-body nph correlations induced by a pairing+quadrupole residual interaction. These occupation numbers have then been used to define a thermal ground state which is the basis of an RPA approach to calculate the capture cross sections, considering only $1p1h$ excitations on the top of this ground state. Therefore the hybrid model does not include explicitly $2p2h$ pairing correlations when calculating strength distributions.

Repeating our observation from above, the TQRPA has two distinct transitions to overcome Pauli blocking. Using, for the sake of simplicity the language of the Independent Particle Model, in the TQRPA GT transitions can occur from a configuration-mixed states with $0p0h$ and $2p2h$ components. These transitions lead to excited states with centroids which are shifted by the excitation energy of two particles which are raised across the pf - sdg shell gap, which corresponds to about 8 MeV for ^{76}Ge . The two peaks observed in the TQRPA GT strength distribution in Fig. 5(a),(b) correspond to these two transitions. As the $2p2h$ component has two neutron holes, GT transitions into these holes are not Pauli blocked. Hence these transitions are relatively strong within the TQRPA model at low temperatures. On the other hand, GT transitions between pure $0p0h$ components are Pauli blocked. Transitions to final states corresponding to the lower centroid are only possible due to the small mixing

of 2p2h configurations into the final states. Hence the GT strength corresponding to the lower peak is rather weak at low temperatures (Fig. 5(b)). The relative weight of the transition strength between these two peaks changes with increasing temperature due to the growing of the thermal excitations and the decreasing correlations induced by pairing. The later effect dominates at modest temperatures. As a consequence, the strength in the upper peak decreases, while the lower peak grows and, at temperatures beyond the critical temperature T_{cr} , dominate the GT strength distribution in the TQRPA model (Fig. 5(d)).

It is found that in the SMMC approach many-body correlations lead to much stronger excitation of particles (mainly neutrons) across the pf - sdg shell gap than found in the TQRPA model. This is demonstrated in Fig. 6(a)-(d), which compares the SMMC and thermal BCS occupation numbers for various orbitals as function of temperature. While BCS predicts only 0.3 neutrons to be excited out of the pf -shell at $T = 0$ for ^{76}Ge , this number is about 1.2 for the SMMC, which is actually also smaller than the number of neutron excitations across the shell gap, derived recently experimentally (2.48 ± 0.30) [44]. Obviously the differences in occupation numbers leads to a larger Pauli unblocking within the SMMC approach than found in TQRPA model. Correspondingly the RPA calculation on top of the SMMC occupation numbers predicts more GT strength in the energy range around 10 MeV (corresponding to the 0p0h centroid in the TQRPA calculation) which, as we will show below, results also in higher capture cross sections at low temperatures. In passing we note that, at low temperatures, the SMMC predicts a larger number of neutron excitations, but a smaller number of proton excitations across the pf - sdg shell gap, than the TQRPA model. This underlines the importance of pn-correlations, induced by isovector pairing and quadrupole interactions in the SMMC approach. Such pn-correlations are not considered in the present TQRPA calculations.

In the SMMC the many-body correlations induced by the pairing+quadrupole interaction also yield a significantly smaller temperature dependence in the occupation numbers than observed in the TQRPA approach. In this model the energies of the unblocked GT_+ transitions essentially depend on temperature: at $T > T_{\text{cr}}$, when unblocking is due to thermal excitations (thermal unblocking), they are smaller than the ones at $T < T_{\text{cr}}$, when unblocking is due to configuration mixing. Obviously, the significant shift of the GT_+ peaks to lower excitation energies favors electron capture. One can conclude that at $T > T_{\text{cr}}$ GT_+ transitions in neutron-rich nuclei are more unblocked than at $T < T_{\text{cr}}$.

To explain the second effect, we consider the total strength for the $j_p \rightarrow j_n$ transition

$$S_t(j_p \rightarrow j_n) = \sum_i \Phi_i(j_p \rightarrow j_n) = (f_{j_p j_n}^1)^2 n_{j_p} (1 - n_{j_n}), \quad (24)$$

where n_{j_τ} is the proton ($\tau = p$) or neutron ($\tau = n$) occupation factor

$$n_j = \langle 0(T); \text{qp} | a_{jm}^\dagger a_{jm} | 0(T); \text{qp} \rangle = u_j^2 y_j^2 + v_j^2 x_j^2. \quad (25)$$

The value of $n_{j_p}(1 - n_{j_n})$ determines the unblocking probability for the $j_p \rightarrow j_n$ transition. As it follows from Eq. (25) the unblocking probability depends on the temperature through the coefficients of both the Bogoliubov and thermal transformation, i.e., it is determined by both configuration mixing and thermal excitations. We note again that at $0 < T < T_{\text{cr}}$ the total strength S_t of the unblocked particle-particle or hole-hole transition is not concentrated in only one peak, but as it follows from (23), is fragmented into four parts. Fig. 6(e),(f) show the unblocking probabilities for the $1f_{7/2}^p \rightarrow 1f_{5/2}^n$ and $1g_{9/2}^p \rightarrow 1g_{7/2}^n$ transitions as a function of temperature.

As seen from the figure the unblocking probabilities for both transitions have a minimum at the critical temperature. It is apparent that this minimum occurs because at T_{cr} pairing correlations vanish while thermal effects are not yet sufficiently strong to occupy the $1g_{9/2}$ proton orbit or unblock the $1f_{5/2}$ neutron orbit. As a result the total transition strength S_t decreases in the vicinity of the critical temperature. In contrast, this minimum is absent in the SMMC unblocking probabilities (see Fig. 6(e),(f)). Here the residual interaction introduces a slight, but gradual increase of the probability with temperature. At $T > 1.5$ MeV the SMMC and TQRPA results converge as is expected in the high temperature limit.

The fact that crossing shell gaps by correlations is a rather slowly converging process which requires the consideration of multi-particle-multi-hole configurations has already been observed in large-scale diagonalization shell model calculations, e.g. studying the calcium isotope shifts [45] or the M1 strength in argon isotopes [46].

For neutron-rich nuclei the contribution of first forbidden $p \rightarrow n$ transitions to electron capture is not negligible [4, 20]. The strength distributions of first-forbidden 0^- , 1^- , and 2^- transitions in ^{76}Ge are shown in Fig. 7 for temperatures $T = 0.2$ and 1.3 MeV. The distributions have been folded by the same procedure used above for the allowed transitions. As is seen from the figure, a temperature increase weakly affects the peaks in the 0^- , 2^- strength distributions. The reason is that these are dominated by particle-hole transitions whose energy depends only weakly on temperature (in contrast to particle-particle and hole-hole transitions). With increasing temperature the peaks slightly shift to lower excitation energies due to the vanishing of the pairing correlations and some transition strength appears below the zero temperature threshold due to thermally unblocked transitions.

Finite temperature induces a significant spread in the 1^- transition strength distribution. The spread can be easily explained. At $T = 0.2$ MeV the main peak in the

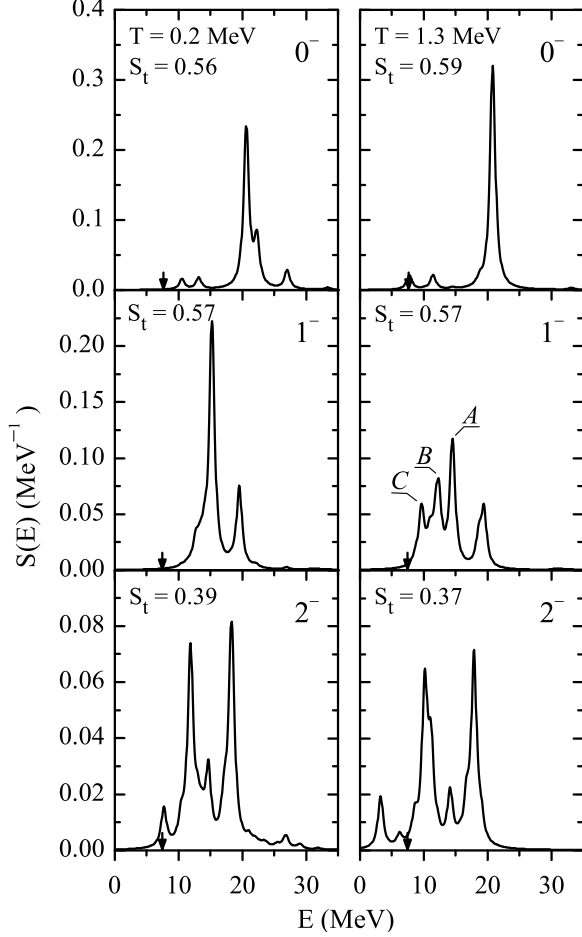


FIG. 7: Folded strength distributions of first forbidden 0^- , 1^- and 2^- $p \rightarrow n$ transitions in ^{76}Ge at $T = 0.2$ MeV (left panels) and $T = 1.3$ MeV (right panels); E is the transition energy. The strength distributions for the 2^- multipole correspond to 25 MeV electrons. S_t is the total strength. The arrows indicate the zero temperature threshold. The letters label the 1^- transitions: $A \equiv 1f_{7/2}^p \rightarrow 2d_{5/2}^n$, $B \equiv 1f_{5/2}^p \rightarrow 1g_{7/2}^n$, $C \equiv 1f_{7/2}^p \rightarrow 1g_{9/2}^n$.

distribution is generated by three single-particle transitions: $1f_{7/2}^p \rightarrow 2d_{5/2}^n$, $1f_{5/2}^p \rightarrow 1g_{7/2}^n$, and $1f_{7/2}^p \rightarrow 1g_{9/2}^n$. The first is a particle-hole transition and its energy depends only slightly on temperature. The second and third ones are particle-particle and hole-hole transitions, respectively. As discussed above, the energies of particle-particle and hole-hole transitions at $T > T_{\text{cr}}$ are noticeably lower than that at $T < T_{\text{cr}}$. Therefore, at $T = 1.3$ MeV, the peak is fragmented into three parts, resulting in a broadening of the 1^- strength distribution. The 1^- peak at $E = 19$ MeV is generated by the particle-hole transition $1f_{7/2}^p \rightarrow 1g_{7/2}^n$ and, hence, its position and strength almost do not depend on the temperature.

To reveal the importance of thermal unblocking for GT_+ transitions in neutron-rich nuclei we perform elec-

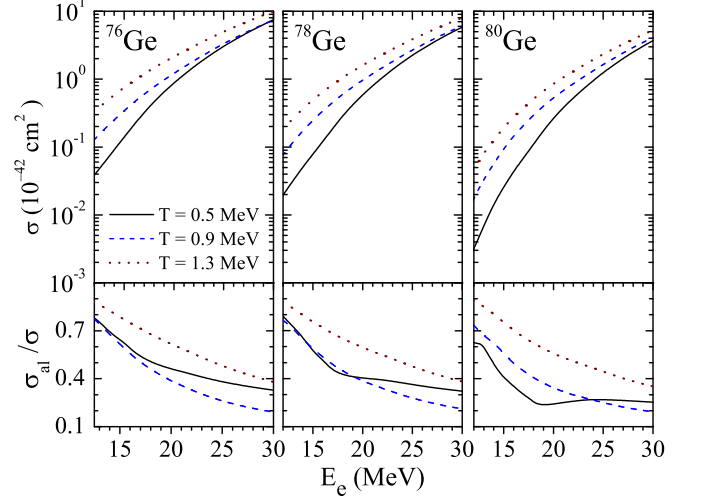


FIG. 8: (Color online) Electron capture cross sections (upper panels) for $^{76,80,80}\text{Ge}$ calculated within the TQRPA approach for various temperatures. Relative contributions of allowed transitions to the electron capture cross sections are shown in the lower panels.

tron capture cross sections calculations. Within the present approach, the total cross section for capture of an electron with energy E_e on a nucleus with charge Z is given by

$$\sigma(E_e, T) = \frac{G_w^2}{2\pi} F(Z, E_e) \sum_{J_i} (E_e - E_{J_i}^{(+)})^2 \Phi_{J_i}^{(+)}, \quad (26)$$

where G_w is the weak interaction coupling constant; $F(Z, E_e)$ is the Fermi function that accounts for the Coulomb distortion of the electron wave function near the nucleus (see, for, example, [9]). Only allowed and first forbidden transitions are involved in the sum over J in the present study.

In Fig. 8 the electron capture cross sections for $^{76,78,80}\text{Ge}$ are shown for three different temperatures. The temperature dependence of the cross sections is most pronounced at moderate electron energies ($E_e \leq 15$ MeV): for $E_e = 15$ MeV a temperature increase from 0.5 MeV to 1.3 MeV results in an enhancement of the cross sections by an order of magnitude. No such enhancement was found in [20] (see below). To make clear the reason of this enhancement, we calculate the relative contribution of allowed transitions to the electron capture cross sections. The results are displayed in the lower part of Fig. 8.

It is seen that at $E_e \leq 15$ MeV electron capture is mainly mediated by allowed transitions. Consequently the cross section enhancement is caused by thermal unblocking of GT_+ transitions (the Fermi contribution to the cross sections is negligible). Furthermore, because of thermal unblocking, the electron energy below which electron capture is dominated by allowed transitions,

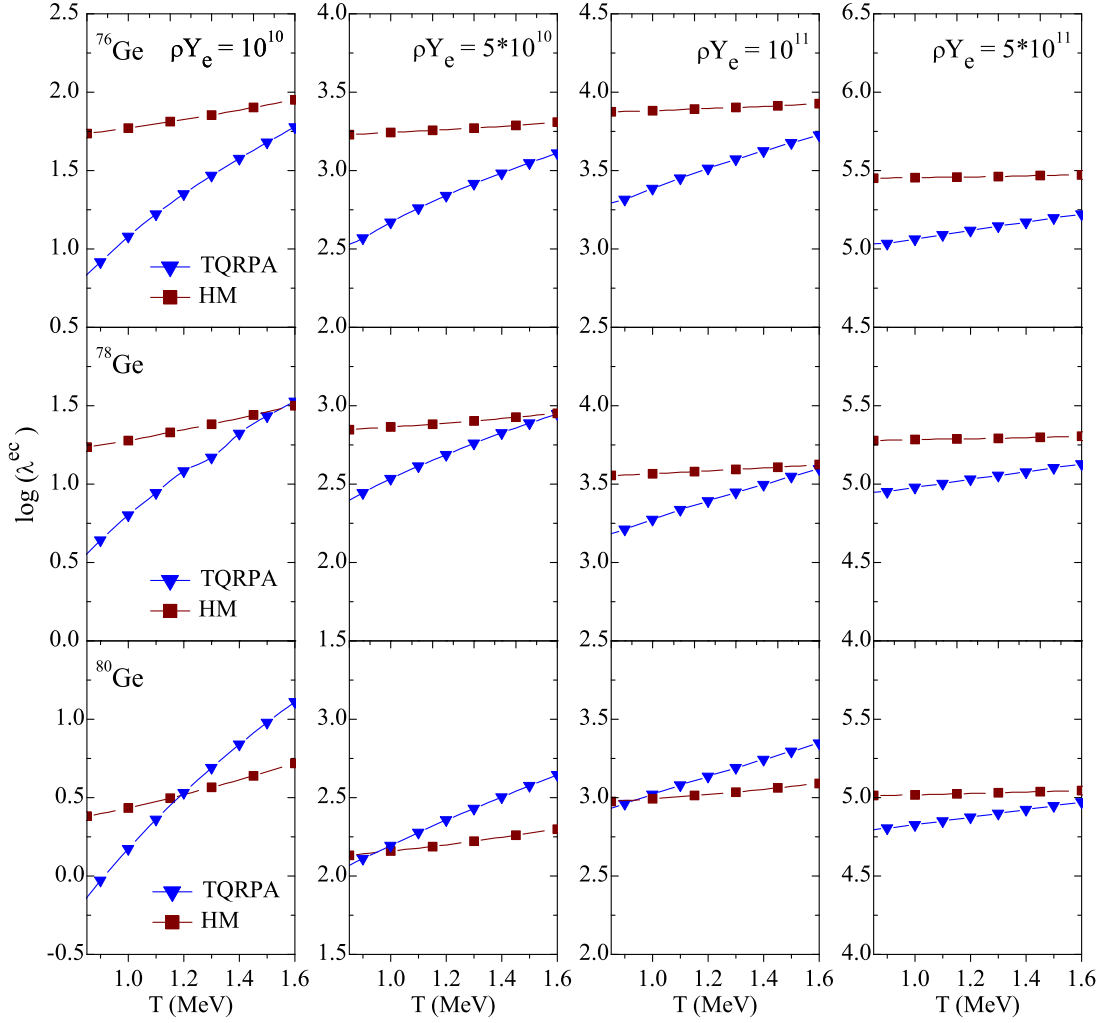


FIG. 9: (Color online) Electron capture rates for $^{76,78,80}\text{Ge}$ calculated using the TQRPA approach as a function of temperature and for selected values of density ρY_e (in g cm^{-3}). For comparison, the rates obtained by the hybrid model are also shown.

shifts to higher values: at $T = 0.5$ and 0.9 MeV this energy is $16 - 18$ MeV, while at $T = 1.3$ MeV it is about 25 MeV. For larger electron energies, the first forbidden transitions become increasingly important. As the strength of the first forbidden transitions is less sensitive to temperature change, the capture cross sections at $E_e \sim 30$ MeV depend only weakly on temperature.

The strong temperature sensitivity of the cross sections at low electron energies reflects the temperature dependence of the TQRPA GT strength distribution, as discussed above. This has mainly two reasons. First, at low temperatures the dominant GT strength resides at larger excitation energies than in the hybrid model. Second, in the TQRPA the GT centroid shifts by several MeV, which is not observed in the hybrid model. Both facts, amplified by the strong phase space energy dependence, lead to a much stronger dependence of the cross

section in the TQRPA model than in the hybrid model. As the GT contribution to the cross sections is larger in the hybrid model than in the present TQRPA calculation, allowed transitions dominate to higher electron energies in the former.

Fig. 9 compares the capture rates for $^{76,78,80}\text{Ge}$ as obtained in the hybrid and the TQRPA models. We note that the hybrid model rates are noticeably larger than the present ones at low temperatures. This is due to the increased unblocking probability in the hybrid model caused by many-body correlations which lead to a larger GT strength at lower excitation energies than in the TQRPA approach. With increasing temperature and density the differences between the rates of the two models become smaller. This has two reasons. At first, with increasing temperature and density the average electron energy increases and the rates become less sensitive to

details of the GT strength distribution. Secondly, the GT strength distributions as calculated in the two models become more similar with increasing temperature as discussed above.

We note that the rates obtained in both models for the temperature and density regime, in which neutron-rich nuclei like those studied here dominate the composition during supernova core collapse ($T > 1$ MeV, $\rho > 5 \times 10^{10}$ g/cm³), are large enough so that electron capture on nuclei dominates over capture on free protons as has been predicted in [20].

VI. CONCLUSION

In this work we have considered the case of GT₊ and first-forbidden transitions in hot nuclei. We have applied the proton-neutron quasiparticle RPA extended to finite temperature by the Thermo-Field-Dynamics formalism. The presented approach allows to treat charge-exchange transitions in nuclei at finite temperature without applying Brink's hypothesis. It fulfills the Ikeda sum rule at finite temperature. As an example, we have calculated the strength distribution for GT₊ transitions in ^{54,56}Fe. We have observed the downward shift of the GT₊ strength with increasing temperature. This shift is caused by vanishing of pairing correlations and the appearance of negative- and low-energy transitions. The shift of the GT₊ strength results in more enhanced electron capture rates at high temperatures as compared to those obtained from shell-model calculations. We have found that the contribution of negative- and low-energy transition, i.e., transitions from thermally excited nuclear states, to electron capture is non-negligible even at low temperatures. We have also calculated the GT₊ strength distribution in the neutron-rich ^{76,78,80}Ge nuclei. It was found that the temperature increase leads to a considerable (of the order of 8 MeV) downward shift of the peaks in the strength distribution and reduces the total transition strength in the vicinity of the critical temperature. This makes the unblocking effect for neutron-rich nuclei quite sensitive to increasing temperature in our model which is clearly observed in the electron capture cross sections and rates for ^{76,78,80}Ge.

If we compare our results to those obtained within the diagonalization shell model for the iron isotopes and within the hybrid SMMC+RPA model for the neutron-rich germanium isotopes, the importance of many-body correlations beyond those induced by pairing in our TQRPA model become apparent. For the isotopes ^{54,56}Fe Pauli unblocking is unimportant as GT transitions are possible even in the Independent Particle Model without correlations. The TQRPA describes the centroid of the GT strength rather well. However, it misses the low-lying GT strength, which is induced by multi-nucleon correlations. Such low-lying strength in ^{54,56}Fe, which is exper-

imentally observed and reproduced by the shell model, is important for calculations of electron capture rates at low temperatures. Its neglect leads to underestimation of the rates.

Pauli unblocking is crucial for the calculation of the GT strength and the associated electron captures rates for the neutron-rich germanium isotopes. Previous diagonalization shell model calculations have shown that such cross-shell effects are rather slowly converging with increasing correlations across the shell gap and require the consideration of many-nucleon correlations. This is in line with the observation that the SMMC approach, which accounts for many-body configuration mixing, recovers significantly more excitations across the *pf*-*sdg* shell gap than is found within the TQRPA approach, which, at low temperatures, derives Pauli unblocking mainly from 2p2h pairing correlations. These differences reflect themselves in different GT distributions and capture rates at low temperatures and densities. However, the two models predict rather similar capture rates for the collapse conditions at which Pauli unblocking matters, making the capture on nuclei dominate over capture on free protons.

In summary, we have presented here a method which allows to calculate stellar electron capture rates at finite temperature in a thermodynamically consistent way. This virtue makes it conceptually superior to the hybrid approach of SMMC+RPA which has previously been used to estimate such rates for neutron-rich nuclei. In the present application of the model we have done a first step towards its complete realization describing correlations within the TQRPA. While this already recovers much of the essential physics, the detailed comparison to shell model results implies that the model must be extended to include correlations beyond TQRPA. This can be achieved by taking into account coupling with complex thermal (e.g., two-phonon) configurations. For charge-exchange excitations in cold nuclei this problem was resolved within the quasiparticle-phonon nuclear model [30, 31] and other approaches [47]. It was found that the coupling with complex configuration strongly affects the RPA strength distribution. As discussed above, the details of the GT strength distribution are of particular importance for weak interaction rates at low densities and temperatures. It is also desirable to extend the approach to more microscopic effective interactions and also to consider the case of deformed nuclei.

Acknowledgments

Discussions with Dr. V. A. Kuzmin are gratefully acknowledged. This work is supported by the Heisenberg-Landau Program, the DFG grant (SFB 634), the Helmholtz Alliance EMMI and HIC for Fair.

-
- [1] M. Di Toro, V. Baran, M. Cabibbo, M. Colonna, A. B. Larionov, and N. Tsoneva, *Phys. Part. Nucl.* **31**, 4333 (2000).
- [2] S. Shlomo and V. M. Kolomietz, *Rep. Prog. Phys.* **68**, 1 (2005).
- [3] K. Langanke and G. Martínez-Pinedo, *Rev. Mod. Phys.* **75**, 819 (2003).
- [4] J. Cooperstein and J. Wambach, *Nucl. Phys. A* **420**, 591 (1984).
- [5] G. M. Fuller, W. A. Fowler, and M. J. Newman, *Astrophys. J. Suppl.* **42**, 447 (1980); **48**, 279 (1982); *Astrophys. J.* **252**, 715 (1982); **293**, 1 (1985).
- [6] M. B. Aufderheide, I. Fushiki, S. E. Woosley, and D. H. Hartmann, *Astrophys. J. Suppl.* **91**, 389 (1994).
- [7] K. Langanke and G. Martínez-Pinedo, *Phys. Lett. B* **436**, 19 (1998).
- [8] K. Langanke and G. Martínez-Pinedo, *Phys. Lett. B* **453**, 187 (1999).
- [9] E. Caurier, K. Langanke, G. Martínez-Pinedo, and E. Nowacki, *Nucl. Phys. A* **653**, 439 (1999); K. Langanke and G. Martínez-Pinedo, *Nucl. Phys. A* **673**, 481 (2000).
- [10] K. Langanke and G. Martínez-Pinedo, *At. Data Nucl. Data Tables* **79**, 1 (2001).
- [11] K. Kar, A. Ray, and S. Sarkar, *Astrophys. J.* **434**, 662 (1994).
- [12] J.-U. Nabi and H. V. Klapdor-Kleingrothaus, *At. Data Nucl. Data Tables* **88**, 237 (2004).
- [13] N. Paar, G. Coló, E. Khan, and D. Vretenar, *Phys. Rev. C* (to be published).
- [14] S. E. Koonin, D. J. Dean, K. Langanke, *Phys. Rep.* **278**, 1 (1997).
- [15] P. B. Radha, D. J. Dean, S. E. Koonin, K. Langanke, and P. Vogel, *Phys. Rev. C* **56**, 3079 (1997).
- [16] A. Juodagalvis, K. Langanke, W. R. Hix, G. Martínez-Pinedo, J. M. Sampaio, [arXiv:0909.0179v1](https://arxiv.org/abs/0909.0179v1) [[nucl-th](https://arxiv.org/abs/0909.0179v1)].
- [17] J. A. Halbleib and R. A. Sorensen, *Nucl. Phys. A* **98**, 542 (1967).
- [18] Y. Takahashi and H. Umezawa, *Collect. Phenom.* **2**, 55 (1975).
- [19] H. Umezawa, H. Matsumoto and M. Tachiki, *Thermo field dynamics and condensed states* (North-Holland, Amsterdam, 1982).
- [20] K. Langanke, E. Kolbe, and D. J. Dean, *Phys. Rev. C* **63**, 032801(R) (2001).
- [21] K. Tanabe, *Phys. Rev. C* **37**, 2802 (1988).
- [22] T. Hatsuda, *Nucl. Phys. A* **492**, 187 (1989).
- [23] O. Civitarese and A. L. DePaoli, *Z. Phys. A* **344**, 243 (1993).
- [24] D. S. Kosov and A. I. Vdovin, *Mod. Phys. Lett. A* **9**, 1735 (1994).
- [25] D. S. Kosov, A. I. Vdovin, and J. Wambach, in *Proceedings of the International Conference on Nuclear Structure and Related Topics, Dubna, 1997*, edited by S. N. Ershov, R. V. Jolos, V. V. Voronov (JINR, Dubna, E4-97-327, 1997), p. 254.
- [26] I. Ojima, *Ann. Phys.* **137**, 1 (1981).
- [27] A. A. Dzhioev and A. I. Vdovin, *Int. J. Mod. Phys. E* **18**, 1535 (2009).
- [28] A. A. Dzhioev, A. I. Vdovin, V. Yu. Ponomarev, and J. Wambach, *Yad. Phys.* **72**, 1373 (2009) [*Phys. At. Nucl.* **72**, 1320 (2009)].
- [29] V. G. Soloviev, *Theory of atomic nuclei: quasiparticles and phonons*, (Institute of Physics Publishing, Bristol and Philadelphia, 1992).
- [30] V. A. Kuzmin and V. G. Soloviev, *J. Phys. G* **10**, 1507 (1984).
- [31] V. A. Kuzmin and V. G. Soloviev, *J. Phys. G* **11**, 603 (1985).
- [32] A. L. Goodman, *Nucl. Phys.* **A352**, 30 (1981).
- [33] O. Civitarese, G. G. Dussel, and R. P. J. Perazzo, *Nucl. Phys. A* **404**, 15 (1983).
- [34] O. Civitarese and M. Reboiro, *Phys. Rev. C* **63**, 034323 (2001).
- [35] A. Heger, S. E. Woosley, G. Martínez-Pinedo, and K. Langanke, *Astrophys. J.* **560**, 307 (2001).
- [36] V. A. Chepurnov, *Yad. Phys.* **6**, 955 (1968) [*Sov. J. Nucl. Phys.* **6**, 696 (1968)].
- [37] K. Pomorski, P. Ring, G. A. Lalazissis, A. Baran, Z. Lojewski, B. Nerlo-Pomorska, and M. Warda, *Nucl. Phys. A* **624**, 349 (1997).
- [38] G. Audi and A. H. Wapstra, *Nucl. Phys. A* **565**, 1 (1993).
- [39] J. Rapaport, T. Taddeucci, T. P. Welch, C. Gaarde, J. Larsen, D. J. Horen, E. Sugarbaker, P. Koncz, C. C. Foster, C. D. Goodman, C. A. Goulding, and T. Masterson, *Nucl. Phys. A* **410**, 371 (1983).
- [40] T. T. Rönqvist, H. Condé, N. Olsson, E. Ramström, R. Zorro, J. Blomgren, A. Håkansson, A. Ringbom, G. Tibell, O. Jonsson, L. Nilsson, P.-U. Renberg, S. Y. van der Werf, W. Unkelbach, and F. P. Brady, *Nucl. Phys. A* **563**, 225 (1993).
- [41] S. El-Kateb, K. P. Jackson, W. P. Alford, R. Abegg, R. E. Azuma, B. A. Brown, A. Celler, D. Frekers, O. Häusser, R. Helmer, R. S. Henderson, K. H. Hicks, R. Jeppesen, J. D. King, G. G. Shute, B. M. Spicer, A. Trudel, K. Raywood, M. Vetterli, and S. Yen, *Phys. Rev. C* **49**, 3128 (1994).
- [42] B. Castel, I. Hamamoto, *Phys. Lett. B* **65**, 27 (1976).
- [43] D. R. Bes, R. A. Broglia, and B. S. Nilsson, *Phys. Rep.* **16**, 1 (1975).
- [44] J. P. Schiffer, S. J. Freeman, J. A. Clark, C. Deibel, C. R. Fitzpatrick, S. Gros, A. Heinz, D. Hirata, C. L. Jiang, B. P. Kay, A. Parikh, P. D. Parker, K. E. Rehm, A. C. C. Villari, V. Werner, and C. Wrede, *Phys. Rev. Lett.* **100**, 112501 (2008).
- [45] E. Caurier, K. Langanke, G. Martínez-Pinedo, F. Nowacki, P. Vogel, *Phys. Lett. B* **522**, 240 (2001).
- [46] A. F. Lisetskiy, E. Caurier, K. Langanke, G. Martínez-Pinedo, P. von Neumann-Cosel, F. Nowacki, A. Richter, *Nucl. Phys. A* **789**, 114 (2007).
- [47] S. Drożdż, V. Klemt, J. Speth, and J. Wambach, *Phys. Lett. B* **166**, 18 (1986); S. Drożdż, F. Osterfeld, J. Speth, J. Wambach, *Phys. Lett. B* **189**, 271 (1987).
- [48] We take into account that the operator $\tilde{Q}_{\lambda\mu}^\dagger = (-1)^{\lambda-\mu} \tilde{Q}_{\lambda-\mu}^\dagger$ transforms under spatial rotations like a spherical tensor of rank λ .
- [49] ^{54}Fe has a closed $1f_{7/2}$ neutron subshell in our single-particle scheme.
- [50] The same effects were found in [28] for ^{80}Ge .